NJC

Accepted Manuscript

This is an *Accepted Manuscript*, which has been through the Royal Society of Chemistry peer review process and has been accepted for publication.

Accepted Manuscripts are published online shortly after acceptance, before technical editing, formatting and proof reading. Using this free service, authors can make their results available to the community, in citable form, before we publish the edited article. We will replace this *Accepted Manuscript* with the edited and formatted *Advance Article* as soon as it is available.

You can find more information about *Accepted Manuscripts* in the Information for Authors.

Please note that technical editing may introduce minor changes to the text and/or graphics, which may alter content. The journal's standard Terms & Conditions and the Ethical guidelines still apply. In no event shall the Royal Society of Chemistry be held responsible for any errors or omissions in this *Accepted Manuscript* or any consequences arising from the use of any information it contains.

ROYAL SOCIETY OF CHEMISTRY

www.rsc.org/njc

Structural Diversity in Aroylthiourea Copper Complexes – Formation and Biological Evaluation of $[Cu(I)(\mu\text{-}S)SCl]_2$, *cis*-$Cu(II)S_2O_2$, *trans*-$Cu(II)S_2O_2$ and $Cu(I)S_3$ cores

Nagamani Selvakumaran[a], Lakshmanan Sandhiya[b], Nattamai S.P. Bhuvanesh[c], Kittusamy Senthilkumar[b], Ramasamy Karvembu[a]*

Copper complexes of the types $[Cu(HL1\text{-}\{\mu\text{-}S\})(HL1\text{-}S)Cl]_2$ (**1**), *cis*-$[Cu(L1\text{-}O,S)_2]$ (**2**), $[Cu(L2\text{-}S)_3]Cl$ (**3**) and *trans*-$[Cu(L2\text{-}O,S)_2]$ (**4**) were synthesized and characterized by analytical, spectroscopic (UV−Vis, FT-IR, NMR / EPR) and single crystal X-ray diffraction techniques. In order to understand the structure, bonding, and band gap of complex **1**, DFT calculations were performed. The computed results revealed that the absorption was associated with ^{1}MLCT transitions while the emission had ^{3}MLCT character. The calculated geometrical parameters agreed well with the experimental values. The binding affinity and binding mode of these copper complexes toward calf thymus (CT) DNA were determined by using UV-Vis spectroscopic titrations and fluorescent indicator displacement (FID) method. These studies showed that the complexes bind in the order of **1**>**2**>**3**>**4** to CT DNA. The protein binding ability has been monitored by the quenching of tryptophan emission in the presence of the complexes using bovine serum albumin (BSA) as a model protein. The copper complexes displayed high cytotoxicity against two cancer cell lines (A549 and MCF7).

Keywords: copper, aroylthiourea, crystal structure, DFT calculation, DNA/BSA binding, cytotoxicity.

[a]Department of Chemistry, National Institute of Technology, Tiruchirappalli-620015, India E-mail: kar@nitt.edu, [b]Department of Physics, Bharathiar University, Coimbatore-641046, India, [c]Department of Chemistry, Texas A & M University, College Station, TX 77842, USA

[†]Electronic supplementary information (ESI) available: Crystallographic data for the structures reported in this paper have been deposited with the Cambridge Crystallographic Data Center (CCDC 980486-980489) as supplementary publication numbers CCDC 980486, CCDC 980487, CCDC 980488 and CCDC 980489 for 1, 2, 3 and 4, respectively. Electronic absorption spectrum of **1**, NMR spectra of **1** and **3**, DNA/protein binding studies of **2**-**4**, DFT calculations tables of **1**, DNA/protein binding and cytotoxicity values. This material is available free of charge via the Internet at http://pubs.rsc.org.

Introduction

The coordination compounds of acylthiourea derivatives display astonishing biological properties such as anticancer, antifungal, antibacterial and antimalarial activities. Nucleic acids and proteins are two of the most imperative biomolecules in any living organism, with the former carrying genetic information and the later implementing and regulating the life processes. DNA is generally the primary intracellular target of anticancer drugs, so the interaction between small molecules and DNA can cause DNA damage in cancer cells, inhibiting the growth of cancer cells and resulting in cell death or apoptosis.[1-5] Bovine serum albumin (BSA) is a major soluble protein of the circulatory system and has many physiological functions, for example it serves as a depot protein for many exogenous compounds.[6,7] Serum albumins found in plasma are important transport proteins and can bind a large variety of bioactive molecules by hydrophobic, hydrophilic and ionic interactions.[8–12] Extensive research on the structure and functions of serum albumins has been carried out by many research groups.[13–15] Significant interaction of any drug with a protein may result in the formation of a stable protein-drug complex which has an important effect on the distribution, metabolism and the efficiency of drugs. So it is essential to find DNA and protein binding agents in order to develop antitumor drugs. We have investigated the DNA and protein binding properties of Ni(II) complexes containing 3,3-dialkyl/aryl-1-(2,4-dichlorobenzoyl)thiourea ligands[16] and self-assembled Ni(II) and Cu(II) metallamacrocycles formed from 3,3,3′,3′-tetrabenzyl-1,1′-aroylbis(thiourea) ligands.[17]

In this paper, we report the results of our investigation on synthesis, characterization, DNA and protein binding properties and cytotoxicity of Cu(I) and Cu(II) complexes containing dichloroaroylthiourea ligands. Interestingly, four structurally different copper complexes were obtained depending on the copper precursors and substituents on the thiourea nitrogen. The reaction of 3,3-diethyl-1-(2,4-dichlorobenzoyl)thiourea (HL1) with copper(II) chloride (2:1) afforded a novel binuclear Cu(I)–Cu(I) complex $[Cu(HL1\text{-}\{\mu\text{-}S\})(HL1\text{-}S)Cl]_2$ (**1**). Accurately, only seven Cu(I)–Cu(I) bond containing Cu_2S_2 core structures were reported.[18–24] Complex **1** is the first binuclear copper(I) complex containing aroylthiourea ligands with Cu–Cu bond. Conversely, in the analogous reaction between 3,3-diisobutyl-1-(2,4-dichlorobenzoyl)thiourea (HL2) and copper(II) chloride, a novel mononuclear trigonal planar complex $[Cu(L2\text{-}S)_3]Cl$ (**3**) was isolated; CuS_3 type of complexes are rare and only six reports (including clusters) are available in the literature.[25–30] However, this is the first report for trigonal planar $Cu(I)S_3$ complex containing aroylthiourea ligands. In addition, reactions

between HL1 / HL2 and copper(II) acetate yielded *cis*-[Cu(L1-O,S)$_2$] (**2**) and *trans*-[Cu(L2-O,S)$_2$] (**4**) respectively. Square planar complexes with aroylthiourea mostly showed *cis* arrangement of the ligands. Only three reports in the literature deal with *trans* coordination of aroylthiourea ligands to the metal center.[31–33]

Experimental section

Materials and Methods

Chemicals were obtained from commercial suppliers (Sigma Aldrich & Merck) and used without further purification. A549 (human lung cancer cell line) and MCF7 (human breast cancer cell line) were purchased from NCCS, Pune for cell culture experiments. Solvents were purified according to the standard procedures. Elemental analyses were carried out on a Vario EL-III elemental analyzer. All the complexes tested have a purity of >95% as determined by elemental analyses. FT-IR spectra were recorded on a Nicolet-iS5 spectrophotometer using KBr pellets. UV-Vis spectra were recorded on a Shimadzu-2600 spectrophotometer operating in the range of 200−800 nm. Emission spectra were recorded on a Jasco V-630 spectrometer using 5% dimethylformamide (DMF) in buffer as the solvent. EPR spectra were recorded with a Brucker ESP 300E X-band spectrometer at 77 K in DMF. NMR spectra were recorded in $CDCl_3$ using TMS as an internal standard on a Bruker 400 MHz spectrometer. Synthesis and crystal structure of the ligands were described in our previous report.[16]

Synthesis of Copper Complexes

[Cu(HL1-{μ-S})(HL1-S)Cl]$_2$ (1): To a methanolic (30 mL) solution of $CuCl_2{\cdot}2H_2O$ (0.1705 g, 0.001 mole), a methanolic solution of 3,3-diethyl-1-(2,4-dichlorobenzoyl)thiourea (HL1) (0.3052 g, 0.002 mole) was added slowly and the mixture was stirred for 3 h at room temperature. The solution was kept at room temperature for 48 h to yield greenish yellow crystals suitable for X-ray diffraction. Yield: 69%. Elemental analyses found: C, 40.58; H, 6.23; N, 7.62; S, 8.90. $C_{48}H_{56}Cl_{10}Cu_2N_8O_4S_4$: Calc. C, 40.63; H, 6.25; N, 7.89; S, 9.04%. UV-Vis (5% DMF in buffer): λ_{max}, nm (ε, $dm^3mol^{-1}cm^{-1}$) 288 (35900), 381 (15800). UV-Vis (solid state): (λ_{max}, nm): 243, 292, 398. FT-IR (KBr, cm^{-1}): 3073 (N–H), 1698 (C═O), 1132 (C═S). ^{1}H NMR (400 MHz, $CDCl_3$): δ, ppm 10.47 (s, 4H), 7.56-7.25 (m, 12H), 3.99-3.37 (m, 16H), 1.38-1.22 (m, 24H). ^{13}C NMR (100 MHz, $CDCl_3$): δ, ppm 179.8 (C═S), 162.6 (C═O), 133.1, 131.9, 131.4, 130.2 (C_6H_5), 49.0 (CH_2−N), 13.2, 11.6 (CH_3).

***cis*-[Cu(L1-O,S)$_2$] (2):** To a methanolic (30 mL) solution of $Cu(OAc)_2{\cdot}H_2O$ (0.1997 g, 0.001 mole), a methanolic solution of 3,3-diethyl-1-(2,4-dichlorobenzoyl)thiourea (HL1) (0.3052 g,

0.001 mole) was added slowly and the mixture was stirred for 3 h at room temperature to yield greenish black crystalline product which was filtered, washed and dried under *vacuum*. The suitable single crystals were grown from DMF solution for X-ray diffraction studies. Yield: 82%. Elemental analyses found: C, 42.74; H, 3.65; N, 8.20; S, 9.52. $C_{24}H_{26}Cl_4CuN_4O_2S_2$: Calc. C, 42.89; H, 3.89; N, 8.34; S, 9.54%. UV-Vis (5% DMF in buffer): λ_{max}, nm (ε, $dm^3mol^{-1}cm^{-1}$) 285 (35500), 378 (12500). UV-Vis (solid state): (λ_{max}, nm): 241, 358, 580. FT-IR (KBr, cm^{-1}): 1502 (C---O), 1200 (C---S). EPR (X band, 77 K, *v* = 9.78 GHz): $g_{\|}$, 2.3020; $g_{\perp}$, 2.1169; $A_{\|}$, 150; $A_{\perp}$, 50; G, 2.6.

[Cu(HL2-S)$_3$]Cl (3): To a methanolic (30 mL) solution of $CuCl_2{\cdot}2H_2O$ (0.1705 g, 0.001 mole), a methanolic solution of 3,3-diisobutyl-1-(2,4-dichlorobenzoyl)thiourea (HL2) (0.3613 g, 0.001 mole) was added slowly and the mixture was stirred for 3 h at room temperature. The solution was kept at room temperature for 48 h to yield greenish yellow crystals suitable for X-ray diffraction. Yield: 62%. Elemental analyses found: C, 48.69; H, 5.42; N, 6.95, S, 8.09. $C_{48}H_{66}Cl_7CuN_6O_3S_3$: Calc. C, 48.74; H, 5.62; N, 7.10; S, 8.13%. UV-Vis (5% DMF in buffer): λ_{max}, nm (ε, $dm^3mol^{-1}cm^{-1}$) 283 (43300), 384 (16700). UV-Vis (solid state): (λ_{max}, nm): 256, 297, 403. FT-IR (KBr, cm^{-1}): 3127 (N–H), 1700 (C═O), 1140 (C═S). ^{1}H NMR (400 MHz, $CDCl_3$): δ, ppm 10.20 (d, *J* = 12 Hz, 3H), 7.59 (d, *J* = 8 Hz, 3H), 7.40 (s, 3H), 7.26 (d, *J* = 8 Hz, 3H), 3.76 (d, *J* = 8 Hz, 6H), 3.40 (d, *J* = 8 Hz, 6H), 2.36-2.20 (m, 6H), 1.03-0.88 (m, 36H). ^{13}C NMR (100 MHz, $CDCl_3$): δ, ppm 179.3 (C═S), 161.9 (C═O), 137.6, 132.8, 132.1, 131.4, 130.2, 127.2 (C_6H_5), 62.5, 60.7 (CH_2–N), 27.8, 26.3 (CH), 20.2, 20.0 (CH_3)

***trans*-[Cu(L2-O,S)$_2$] (4):** To a methanolic (30 mL) solution of $Cu(OAc)_2{\cdot}H_2O$ (0.1997 g, 0.001 mole), a methanolic solution of 3,3-diisobutyl-1-(2,4-dichlorobenzoyl)thiourea (HL2) (0.3613 g, 0.001 mole) was added slowly and the mixture was stirred for 3 h at room temperature to yield green coloured solid product which was filtered, washed and dried under *vacuum*. The suitable single crystals were grown by slow evaporation method from the DMF solution at room temperature. Yield: 78%. Elemental analyses found: C, 48.97; H, 5.30; N, 7.01; S, 8.04. $C_{32}H_{42}Cl_4CuN_4O_2S_2$: Calc. C, 49.01; H, 5.39; N, 7.14; S, 8.18%. UV-Vis (5% DMF in buffer): λ_{max}, nm (ε, $dm^3mol^{-1}cm^{-1}$) 286 (32600), 369 (14600). UV-Vis (solid state): (λ_{max}, nm): 243, 342, 641. FT-IR (KBr, cm^{-1}): 1489 (C---O), 1229 (C---S). EPR (X band, 77 K, *v* = 9.78 GHz): $g_{\|}$, 2.2379; $g_{\perp}$, 2.0263; $A_{\|}$, 185; $A_{\perp}$, 42; G, 4.5.

Crystal Structure Determination

A Bruker Gadds (Cu Kα) or Bruker Apex 2 (Mo Kα) X-ray (three-circle) diffractometer was employed for crystal screening, unit cell determination, and data collection. Integrated intensity information for each reflection was obtained by reduction of the data frames with APEX2.[34] The integration method employed a three dimensional profiling algorithm and all data were corrected for Lorentz and polarization factors, as well as for crystal decay effects. Finally the data were merged and scaled to produce a suitable data set. SADABS[35] was employed to correct the data for absorption effects. A solution was obtained readily using SHELXTL (SHELXS).[36] Hydrogen atoms were placed in idealized positions and were refined using a riding model. All non-hydrogen atoms were refined with anisotropic thermal parameters. The structure was refined (weighted least squares refinement on F^2) to convergence.[37,38] Platon was used to verify the absence of additional symmetry and voids. OLEX2 was employed for the structure plots.[38] The crystal data and refinement details of complexes (**1, 2, 3** and **4**) are listed in Tables 1 and 2.

Computational Methodology

The geometry of the singlet ground state (S_0) and the lowest triplet state (T_1) of complex **1** is optimized using DFT-B3LYP method.[39,40] The effective core potential (ECP) basis set LACV3P is used for Cu atom and 6-311G(d,p) basis set is used for all the other atoms. The LACV3P basis set is a triple-zeta contraction of the LACVP [74] ECP basis set available in Jaguar program.[41] These fully optimized stationary points are further characterized by harmonic vibrational frequency analysis to ensure that the structures are minima on the potential energy surface (PES). The net atomic charges of the studied complex are calculated using Natural Population Analysis (NPA). In addition, the structure of the singlet ground state (S_0) and triplet state (T_1) of complex **1** is optimized using the meta hybrid DFT method, M06-2X functional with LACV3P basis set. The M06-2X functional has been proved to include dispersion interactions in an effective way.[42,43] All the electronic structure calculations were performed using Gaussian 09 program package.[44]

DNA and Protein Binding Experiments

DNA and protein experiments were described in our previous report.[17]

MTT Assay

MTT [3-(4,5-dimethylthiazole-2-yl)-2,5-diphenyl tetrazolium] assay was performed to evaluate the viability of the cells due to the effect of the samples tested and it is a colorimetric test based on the selective ability of the viable cells to reduce the tetrazolium component of

MTT into purple colored formazan crystals. Four different dilutions were prepared by dilution with DMSO and media. To test the biocompatibility of the samples, cells were seeded at a density of 10,000 cells/well into a 96 well plate. After attaining 90% confluency, the cells were incubated with different concentrations of the samples for a period of 24 h. Cells in media alone devoid of test samples acted as a positive control and wells treated with cyclophosphamide (1%) functioned as a negative control. The cells were incubated with MTT solution for 4 h followed by 1 h incubation with solubilisation buffer. Then the absorbance of the solution was measured at a wavelength of 570 nm using a Beckmann Coulter Elisa plate reader (BioTek Power Wave XS).[45] Triplicate samples were analyzed for each experiment. Cell viability was expressed as the percentage of the negative control calculated as, viability (%) = (Nt / Nc) × 100; Nt is the absorbance of the cells treated with sample and Nc is the absorbance of the untreated cells.

Results and discussion

Synthesis of the Complexes

The reaction of 3,3-diethyl-1-(2,4-dichlorobenzoyl)thiourea (HL1) with copper(II) chloride (2:1) afforded a novel binuclear Cu(I)–Cu(I) complex $[Cu(HL1\text{-}\{\mu\text{-}S\})(HL1\text{-}S)Cl]_2$. This is the first binuclear Cu(I) complex containing aroylthiourea ligands with Cu–Cu bond. When similar reaction was carried out with 3,3-diisobutyl-1-(2,4-dichlorobenzoyl)thiourea (HL2), the rare trigonal planar complex $[Cu(L2\text{-}S)_3]Cl$ was isolated. During the synthesis of **1** and **3** copper was reduced from Cu(II) to Cu(I). In many syntheses of copper complexes, irreversible Cu(II)/Cu(I) redox was observed.[46] Cu(II) is a borderline hard acid showing the characteristics of both hard and soft classes of metals, usually has either five or six coordination sites, tends to form colorful, paramagnetic complexes, and is a weak oxidant that binds thiourea, CN^-, SO_3^{2-}, dithizone and π-acids. Binding ligands such as these generates thermodynamic conditions that promote the reduction of Cu(II) to Cu(I). Reactions of HL1 and HL2 with $Cu(OAc)_2{\cdot}H_2O$ resulted in the formation of *cis*-$[Cu(L1\text{-}O,S)_2]$ (**2**) and *trans*-$[Cu(L2\text{-}O,S)_2]$ (**4**) respectively (Scheme 1). All the complexes were isolated from the methanol solution and well characterized by analytical, spectral and single crystal XRD techniques.

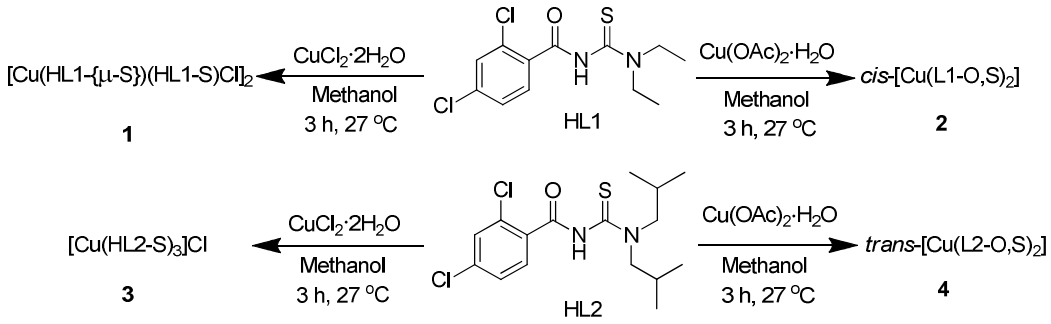

Scheme 1 Synthesis of Cu complexes.

Characterization of the Complexes

The solid state electronic spectra of **2** and **4** demonstrated a broad band at 584 and 641 nm respectively, which were allocated to d → d transition of the Cu(II) ions. This d → d transition is typical of a square planar Cu(II) ion.[47] The electronic spectra of **1** and **3** did not show d → d transition band, which designates d^{10} configuration or diamagnetic nature of **1** and **3**. The intra ligand and the metal to ligand charge transfer transitions of **1**−**4** were perceived in the regions 241-256 and 286-403 nm respectively. The electronic spectra of the complexes recorded in solution state by dissolving them in 5% DMF in buffer showed two bands in the regions 283-286 and 369-384 nm, which were assigned to intra ligand and charge transfer (M → L) transitions, respectively. The absorption spectrum of **1** (Fig. †S1) has shown the identical bands in pure DMF solution, indicates that the complex is unchanged in the Tris-HCl buffer solution. Both the Cu(I) and Cu(II) complexes presented MLCT band in the same range. This may be due to the fact that the Cu(I) and Cu(II) complexes are distorted which exemplifies a compromise between tetrahedral/trigonal Cu(I) and square planar Cu(II). This arrangement at the metal center resembles transition state geometry between tetrahedral and square planar, and permits similar MLCT in Cu(I) and Cu(II) complexes.[48]

The characteristic FT-IR absorption bands of the complexes were compared with that of the ligands. The ligands HL1 and HL2 showed an intense band at 1654 and 1701 cm^{-1} respectively for C═O stretching. This band was shifted to lower frequency (1489 and 1502 cm^{-1} for **2** and **4** respectively) after complexation. A medium intensity band due to C═S stretching appeared at 1245 and 1257 cm^{-1} for HL1 and HL2 respectively was also found to be shifted towards lower frequency value (1200 and 1229 cm^{-1}). In addition, the N–H stretching frequency was disappeared in the FT-IR spectra of **2** and **4**. These facts

recommend that HL1 and HL2 act as monobasic bidentate ligands and coordinated to Cu(II) metal center *via* S and O atoms in complexes **2** and **4**. In the FT-IR spectra of **1** and **3**, position of bands due to N–H and C═O stretching was unchanged compared to the ligands, while the band due to C═S vibration was shifted to lower frequency (1132 cm^{-1} for **1** and 1140 cm^{-1} for **3**), suggesting neutral monodentate coordination of the ligand *via* S to Cu(I) center in both the cases.[49]

The signal of the N–H proton was observed as singlet at δ 8.45 and 8.65 ppm in the ^{1}H NMR spectra of ligands HL1 and HL2 respectively, which was observed in the downfield region at δ 10.47 and 10.20 ppm in that of copper complexes **1** and **3** respectively, indicates the interaction of N–H proton with Cl^{-} (N–H····Cl) in both the cases and also non involvement of N–H group in coordination. It is clear from NMR that **1** and **3** exhibit identical structure in solid as well as in solution state (Fig.s †S2 and †S3). The resonances of aromatic and aliphatic protons of the ligands were appeared at δ 7.32-7.62 and δ 0.91-3.98 respectively. The signals due to aromatic (δ 7.35-7.59) and aliphatic (δ 0.88-3.99) protons did not undergo a significant shift in the copper(I) complexes. In the ^{13}C NMR spectra of the complexes, carbonyl and thiocarbonyl carbon signals were observed in the regions δ 161.9-162.6 and 179.3-179.8 ppm respectively (Fig.s †S4 and †S5). These resonances are comparable with that of corresponding ligands (HL1 and HL2; δ 161.3-162.2 and δ 177.9-179.1). The resonances due to aliphatic (δ 11.6-62.5) and aromatic (δ 127.2-137.6) carbons in complexes **1** and **3** did not show any significant change compared with their corresponding ligands (δ 11.4-61.7 and 127.7-138.1 ppm).

The X-band EPR spectra of **2** and **4** in the frozen state (DMF) are shown in Fig. 1. A square based chromophore is expected to show a $g_{\parallel}$ value of 2.200 and $A_{\parallel}$ value in the range 180-200 G. Any distortion from the planarity of square planar geometry would increase the $g_{\parallel}$ and decrease the $A_{\parallel}$ values.[50] The observed values of $g_{\parallel}$ (2.3020) and $A_{\parallel}$ (150 G) for **2** are consistent with significant distortion from planarity, which is also evident from the X-ray crystal structure of **2**. The values of $g_{\parallel}$ (2.2379) and $A_{\parallel}$ (185 G) for complex **4** propose perfect square planar geometry around Cu(II).

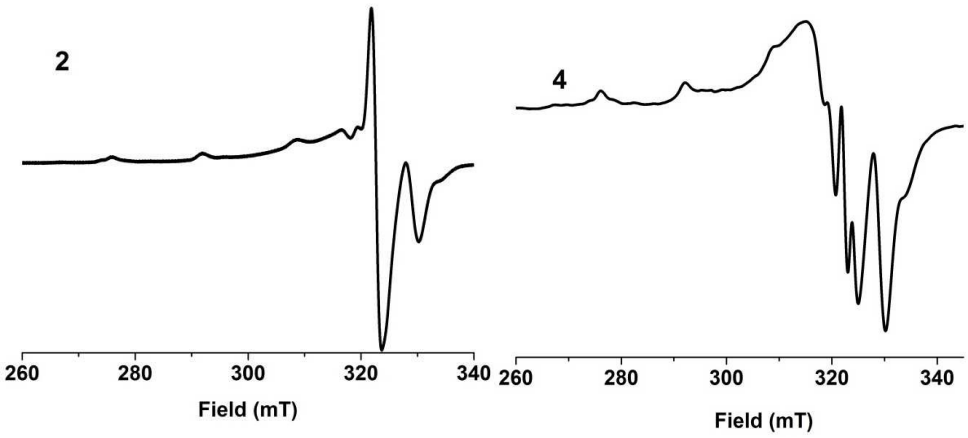

Fig. 1 X-Band EPR spectra of **2** and **4** in solution state at 77 K, v = 9.78 GHz.

Description of the Crystal Structures of 1–4

The crystal data and refinement details of **1**–**4** are listed in Tables 1 and 2. The thermal ellipsoidal plot of **1**–**4** including atom numbering scheme is shown in Figs. 2-5. The selected bond lengths and bond angles are given in Tables 3 and 4.

Table 1 Crystal data and structure refinement for **1** and **3**.

Complex	**1**	**3**
Empirical formula	$C_{48}H_{56}Cl_{10}Cu_2N_8O_4S_4$	$C_{48}H_{66}Cl_7CuN_6O_3S_3$
Formula weight	1418.83	1182.93
Temperature (K)	110.15 K	110.15 K
Wavelength (Å)	1.54178 Å	0.71073 Å
Crystal system	Triclinic	Trigonal
Space group	*P*-1	*R*-3
Unit cell dimensions		
a (Å)	9.1070(6)	13.7134(10)
b (Å)	13.0905(9)	13.7134(10)
c (Å)	25.3601(18)	53.180(7)
α (°)	85.276(5)	90
β (°)	82.088(3)	90
γ (°)	84.915(4)	120
Volume (Å^3)	2975.2(4)	8661.1(17)
Z	2	6
Density (calculated)	1.584 Mg/m^3	1.361 Mg/m^3
Absorption coefficient	6.734 mm^{-1}	0.854 mm^{-1}
F(000)	1448	3696
Crystal size (mm^3)	0.08 × 0.06 × 0.05	0.12 × 0.09 × 0.05
θ range for data collection (°)	1.76 to 60.00	1.88 to 27.50

Index ranges	-10<=*h*<=10, -14<=*k*<=14, -28<=*l*<=28	-17<=*h*<=17, -17<=*k*<=17, -69<=*l*<=69
Reflections collected	28316	32670
Independent reflections	8355 [R(int) = 0.0570]	4440 [R(int) = 0.0554]
Completeness to θ = 27.49°/60 °	94.6 %	99.9 %
Absorption correction	Semi-empirical from equivalents	Semi-empirical from equivalents
Max. and min. transmission	0.7295 and 0.6149	0.9585 and 0.9044
Refinement method	Full-matrix least-squares on F^2	Full-matrix least-squares on F^2
Data/restraints/parameters	8355 / 0 / 693	4440 / 19 / 234
Goodness-of-fit on F^2	0.960	1.031
Final R indices [I>2σ(*I*)]	R1 = 0.0370, wR2 = 0.0958	R1 = 0.0438, wR2 = 0.1043
R indices (all data)	R1 = 0.0461, wR2 = 0.1002	R1 = 0.0581, wR2 = 0.1148
Largest diff. peak and hole (e.Å^{-3})	0.77 and -0.75	0.90 and -0.75

Table 2 Crystal data and structure refinement for **2** and **4**.

Complex	**2**	**4**
Empirical formula	$C_{24}H_{26}Cl_4CuN_4O_2S_2$	$C_{32}H_{42}Cl_4CuN_4O_2S_2$
Formula weight	671.95	784.15
Temperature (K)	110.15 K	150.15 K
Wavelength (Å)	1.54178 Å	0.71073 Å
Crystal system	Triclinic	Monoclinic
Space group	*P*-1	$P2_1/c$
Unit cell dimensions		
a (Å)	8.5233(6)	9.887(4)
b (Å)	13.2721(9)	19.632(7)
c (Å)	13.6992(9)	10.330(4)
α (°)	70.310(4)	90
β (°)	82.388(4)	111.326(4)
γ (°)	74.666(4)	90
Volume (Å^3)	1405.52(17)	1867.9(12)
Z	2	2
Density (calculated)	1.588 Mg/m^3	1.394 Mg/m^3
Absorption coefficient	6.239 mm^{-1}	1.017 mm^{-1}
F(000)	686	814
Crystal size (mm^3)	0.12 × 0.08 × 0.01	0.22 × 0.18 × 0.10

θ range for data collection (°)	3.43 to 60.00	2.75 to 27.50
Index ranges	-9<=*h*<=9, -14<=*k*<=14, -15<=*l*<=15	-12<=*h*<=12, -25<=*k*<=25, -13<=*l*<=13
Reflections collected	27960	21274
Independent reflections	4077 [R(int) = 0.0695]	4278 [R(int) = 0.0310]
Completeness to θ = 27.49°/60°	97.8 %	99.7 %
Absorption correction	Semi-empirical from equivalents	Semi-empirical from equivalents
Max. and min. transmission	0.9402 and 0.5214	0.9052 and 0.8073
Refinement method	Full-matrix least-squares on F^2	Full-matrix least-squares on F^2
Data / restraints / parameters	4077 / 0 / 339	4278 / 0 / 209
Goodness-of-fit on F^2	1.132	1.049
Final R indices [I>2σ(*I*)]	R1 = 0.0393, wR2 = 0.1012	R1 = 0.0288, wR2 = 0.0747
R indices (all data)	R1 = 0.0419, wR2 = 0.1023	R1 = 0.0322, wR2 = 0.0772
Largest diff. peak and hole (e.Å^{-3})	0.52 and -0.65	0.75 and -0.68

Table 3 Selected bond lengths (Å) and angles (°) of **1** and **3**.

1		**3**	
Cu(1)–S(1)	2.2946(10)	Cu(1)−S(1)#2	2.2479(6)
Cu(1)–Cl(3)	2.3257(9)	Cu(1)−S(1)	2.2479(6)
Cu(1)–S(1D)	2.3470(9)	S(1)−C(1)	1.695(2)
Cu(1)–S(1F)	2.4099(9)	O(1)−C(2)	1.211(3)
Cu(1)–Cu(2)	2.6696(7)	N(1)−C(2)	1.380(3)
S(1)–C(1)	1.696(3)	N(1)−C(1)	1.398(3)
N(1)–C(2)	1.369(4)	N(2)−C(1)	1.320(3)
N(1)–C(1)	1.423(4)	N(2)−C(9)	1.474(3)
S(1D)−C(1D)	1.708(3)	S(1)#1−Cu(1)−S(1)#2	118.159(9)
S(1)−Cu(1)−Cl(3)	119.11(3)	S(1)#1−Cu(1)−S(1)	118.163(9)
S(1)−Cu(1)−S(1D)	116.84(3)	S(1)#2−Cu(1)−S(1)	118.163(9)

Cl(3)−Cu(1)−S(1D)	98.67(3)	C(1)−S(1)−Cu(1)	108.67(8)
S(1)−Cu(1)−S(1F)	98.63(3)	C(2)−N(1)−C(1)	124.7(19)
Cl(3)−Cu(1)−S(1F)	111.51(3)		
S(1D)−Cu(1)−S(1F)	112.79(3)		
S(1)−Cu(1)−Cu(2)	122.61(3)		
Cl(3)−Cu(1)−Cu(2)	118.04(3)		
S(1D)−Cu(1)−Cu(2)	57.79(2)		
S(1F)−Cu(1)−Cu(2)	54.99(2)		

#1-y, 1+x-y, +z #2 +y-x, 1-x, +z symmetry transformations used to generate equivalent atoms.

Table 4 Selected bond lengths (Å) and angles (°) of **2** and **4**.

2		**4**	
Cu(1)−O(2)	1.9246(18)	Cu(1)−O(1)	1.9118(13)
Cu(1)−O(1)	1.9431(18)	Cu(1)−O(1)#1	1.9118(13)
Cu(1)−S(2)	2.2299(8)	Cu(1)−S(1)	2.2554(8)
Cu(1)−S(1)	2.2714(7)	Cu(1)−S(1)#1	2.2554(8)
S(1)−C(2)	1.740(3)	Cl(1)−C(4)	1.7333(17)
O(1)−C(1)	1.267(3)	Cl(2)−C(6)	1.7412(17)
N(1)−C(1)	1.313(3)	S(1)−C(2)	1.7261(16)
N(1)−C(2)	1.351(3)	O(1)−C(1)	1.2617(18)
N(2)−C(2)	1.325(3)	N(1)−C(1)	1.319(2)
O(2)−Cu(1)−O(1)	85.28(8)	N(1)−C(2)	1.3540(19)
O(2)−Cu(1)−S(2)	93.50(6)	N(2)−C(2)	1.3393(19)
O(1)−Cu(1)−S(2)	171.86(6)	O(1)−Cu(1−O(1)#1	180.0
O(2)−Cu(1)−S(1)	176.72(6)	O(1)−Cu(1)−S(1)	94.10(3)
O(1)−Cu(1)−S(1)	92.75(6)	O(1)#1−Cu(1)−S(1)	85.90(3)
S(2)−Cu(1)−S(1)	88.82(3)	O(1)−Cu(1)−S(1)#1	85.90(3)

C(2)−S(1)−Cu(1)	100.72(9)	O(1)#1−Cu(1)−S(1)#1	94.10(3)
C(14)−S(2)−Cu(1)	108.15(9)	S(1)−Cu(1)−S(1)#1	180.0
C(1)−O(1)−Cu(1)	129.40(17)	C(2)−S(1)−Cu(1)	106.46(5)
C(13)−O(2)−Cu(1)	131.13(17)	C(1)−O(1)−Cu(1)	132.05(10)
C(1)−N(1)−C(2)	124.0(2)	C(1)−N(1)−C(2)	125.37(13)

#1 -x, -y+1, -z symmetry transformations used to generate equivalent atoms.

[Cu(HL1-{μ-S})(HL1-S)Cl]$_2$ (1): The two Cu(I) centers are in a pseudo tetrahedral environment created by four 3,3-diethyl-1-(2,4-dichlorobenzoyl)thiourea (HL1) ligands and two chloride moieties. There are two terminal and two bridged HL1 ligands and all of them coordinated to Cu(I) *via* neutral S atom. The distance between two Cu centers is 2.6696(7) Å, which indicates the presence of a Cu–Cu bond.[18–24] The two Cu(I) ions and the bridging sulphur atoms lie in a plane forming a Cu_2S_2 core with two short and two long Cu–S bonds. Comparing the C═S bond length of **1** with that of HL1 [C═S, 1.6670(13) Å], there was a considerable elongation of the bond in the complex. Further, C═S bond distance in the bridged ligands is greater than that in the terminal ligands. The τ_4 value usually ranges from 1.00 for a perfect tetrahedral geometry, to zero for a perfect square planar geometry and is 0.55–0.56 for a distorted tetrahedral. The calculated τ_4 values of [Cu(HL1-{μ-S})(HL1-S)Cl]$_2$ are 0.88 and 0.85, which indicate pseudotetrahedral geometry around both the Cu(I) ions.[51,52]

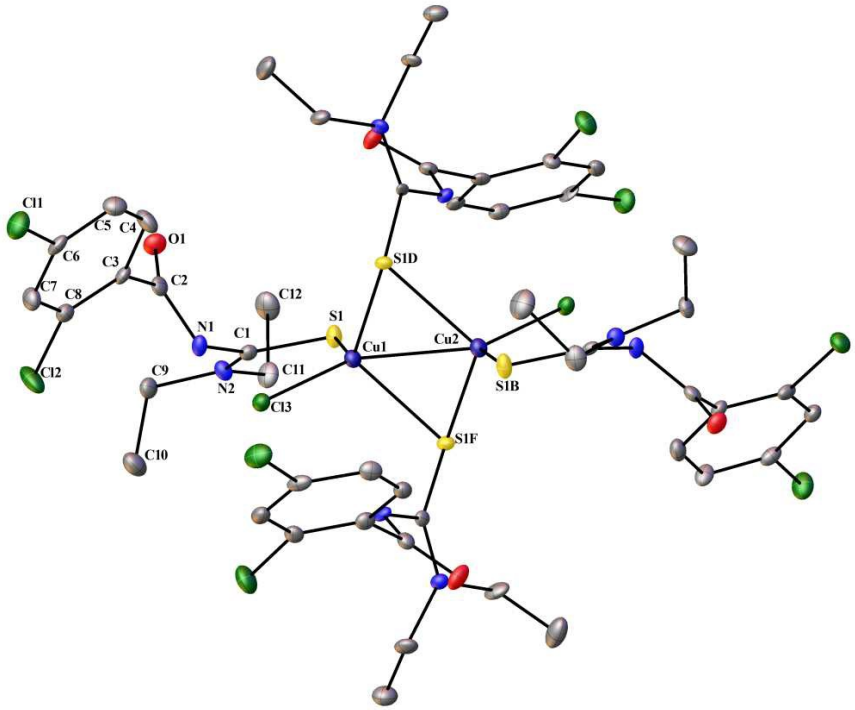

Fig. 2 Thermal ellipsoidal plot of **1** (50 % probability;
Only selected atoms are labeled for clarity).

***cis*-[Cu(L1-O,S)$_2$] (2):** Structural analysis revealed that **2** has a distorted square planar geometry with a *cis*-CuO_2S_2 chromophore, in which two molecules of HL1 coordinated to Cu(II) ion as monoanionic bidentate ligand. The C–O [1.9431(18) and 1.9246(18) Å] and C–S [2.2714 and 2.2299 Å] bond lengths of **2** were considerably more than those in HL1 [C–O, 1.2283(14) Å and C–S, 1.6670(13) Å]. On the other hand, N–C(O) [1.313(3) and 1.323(4) Å] and C(S)–N [1.351(3) and 1.338(4) Å] bonds of the chelate rings in **2** were short compared to the N–C(O) and C(S)–N bond distances of the corresponding ligand [1.3486(15) and 1.4343(15) Å respectively]. These results are consistent with the coordination of the ligands to Cu(II) ion *via* O and S donor atoms. The value of τ_4 (0.117) reveals the distorted square planar geometry for **2**. The sum of the six inter bond angles [53–55] for **2** is 709°, which deviates from an ideal angle of 720°, also suggesting distorted square planar geometry around Cu(II) ion. The coordination geometry and bonding characteristics of **2** are similar to those of already reported Ni(II) aroylthiourea complexes.[16]

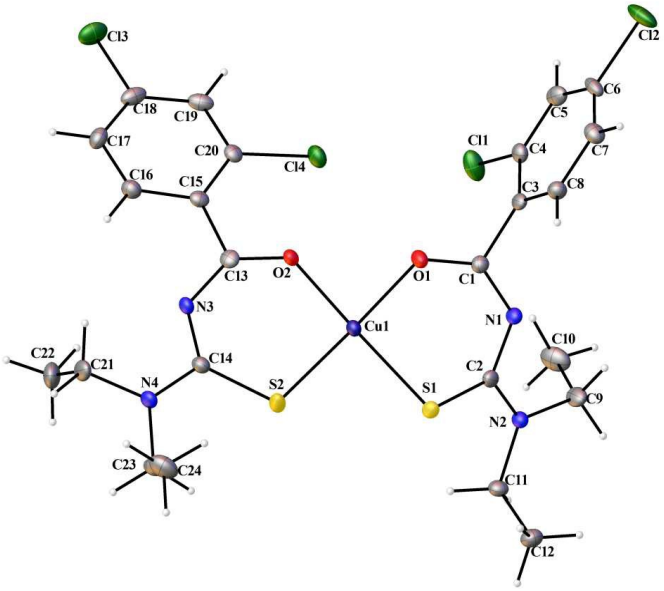

Fig. 3 Thermal ellipsoidal plot of **2** (50 % probability; Hydrogen atoms are not labeled for clarity).

[Cu(HL2-S)$_3$]Cl (3): As presented in Fig. 4, Cu(I) ion in **3** is trigonally coordinated by sulphur atoms of three 3,3-diisobutyl-1-(2,4-dichlorobenzoyl)thiourea (HL2) ligands with equal Cu–S distances [Cu–(S1)#1, Cu–(S1)#2 or Cu–(S1) = 2.2479(6) Å]. The sum of the three inter bond angles is 355° [S(1)#1-Cu-(S1)#2 = 118.159(9)°, S(1)#1-Cu–(S1) = 118.163(9)° and (S1)#2-Cu–(S1) = 118.163(9)°], which slightly deviates from the regular triangle value of 360°, suggesting distorted trigonal planar structure for the complex. Comparing the C–S and C–O bond lengths of **3** with HL2 [C–S = 1.6819(12) Å and C–O = 1.2107(15) Å], there was a slight elongation in the C–S bond length [1.695(2) Å] while C–O bond length remained the same [1.211(3) Å]. On the other hand, N–C bond distances in complex **3** [1.380(3) and 1.398(3) Å] and in HL2 [1.3906(15) and 1.4057(15) Å] were almost same. These results are consistent with the fact that HL2 coordinated to Cu(I) ion through neutral S atom. Formation of intramolecular hydrogen bonds between Cl and N–H [N(1)–H(1), N(1A)–H(1A) and N(1B)–H(1B)] evidently stabilized the molecular structure.

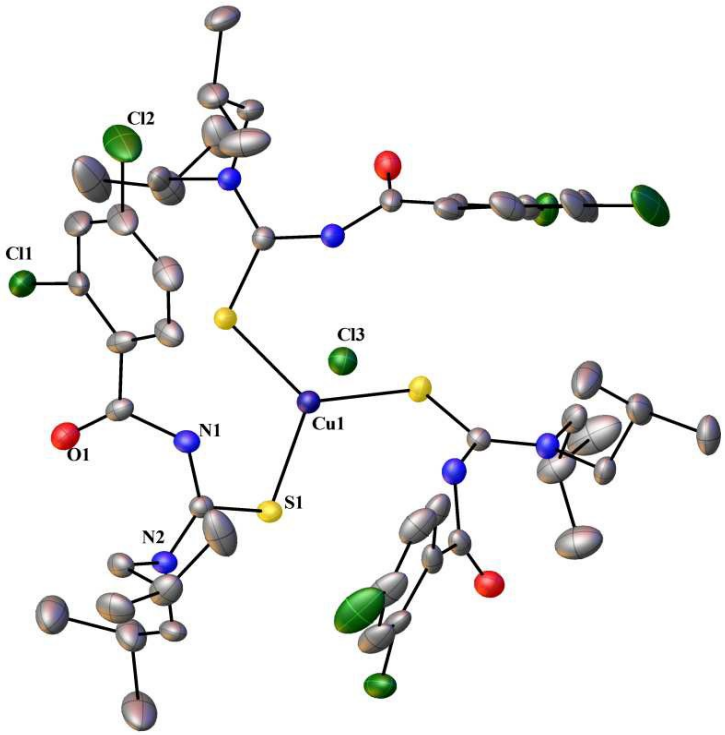

Fig. 4 Thermal ellipsoidal plot of **3** (50 % probability; Only selected atoms are labeled for clarity).

***trans*-[Cu(L2-O,S)$_2$] (4):** The molecular structure of **4** is very similar to that of **2** except the *trans* orientation of the ligands in **4** (Fig. 5). The O(1)–Cu(1)–O(1)# and S(1)–Cu(1)–S(1)# bond angles are equal to 180°. This indicates that the ligands coordinated to Cu(II) through O and S donors which are *trans* to each other. The chelate rings of complex **4** possess short N–C bonds [1.319(2) and 1.3540(19) Å] compared to the corresponding ligand [1.3906(15) and 1.4057(3) Å]. This may be due to the existence of conjugation [O(1)–C(1)–N(1)–C(2)–S(1)] in **4**. These results revealed the deprotonation of N–H prior to coordination. The sum of the six inter bond angles for **4** is 720°, which is equal to an ideal value suggesting perfect square planar geometry around Cu(II). This is also confirmed by the structural index value (τ_4) of 0.

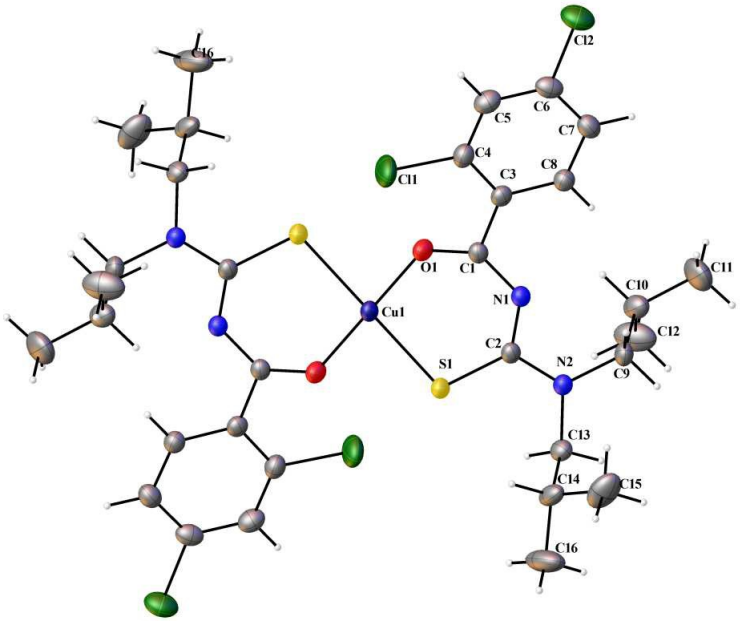

Fig. 5 Thermal ellipsoidal plot of **4** (50 % probability;
Hydrogen atoms and symmetry related atoms are not labeled for clarity).

Theoretical Analysis of Complex 1

The Geometries and Energies of Complex 1: The selected geometrical parameters of complex **1** optimized at B3LYP and M06-2X levels, and X-ray diffraction data are given in Table †S1. The optimized structure of the complex is shown in Fig. 6. From Table †S1, it has been observed that the S_0 state optimized geometrical parameters of the complex are in agreement with the corresponding experimental values and the slight discrepancy comes from the crystal lattice distortion existing in the real molecules. Also, the optimized geometries of the complex in both S_0 and T_1 states do not show significant differences in the coordination sphere around the metal centers. As shown in Fig. 6, the Cu(I) atoms adopt a pseudo tetrahedral coordination geometry. The distance between the Cu centers is 2.75 and 2.98 Å in the singlet and triplet states, respectively at B3LYP level, whereas at the M06-2X level, the Cu–Cu distance is about 0.09 Å higher than that calculated at B3LYP level. The calculated B3LYP and M06-2X bond parameters are comparable within 0.1 Å except for few geometrical changes. The distance between the Cu centers in the singlet state is significantly shorter than that in the dicopper(II) cores, which is about 3 Å.[56] This is due to the presence of bridging sulfur ligands. It is worth to note that, in the singlet state Cu1–S1 and Cu2–S2 bonds are shorter than the Cu1–S3 and Cu2–S4 bonds in the bridging position. Our calculations clearly reveal that the energy of the S_0 state is about 48 and 65 kcal/mol, respectively at

B3LYP and M06-2X levels lower than that of the T_1 state.

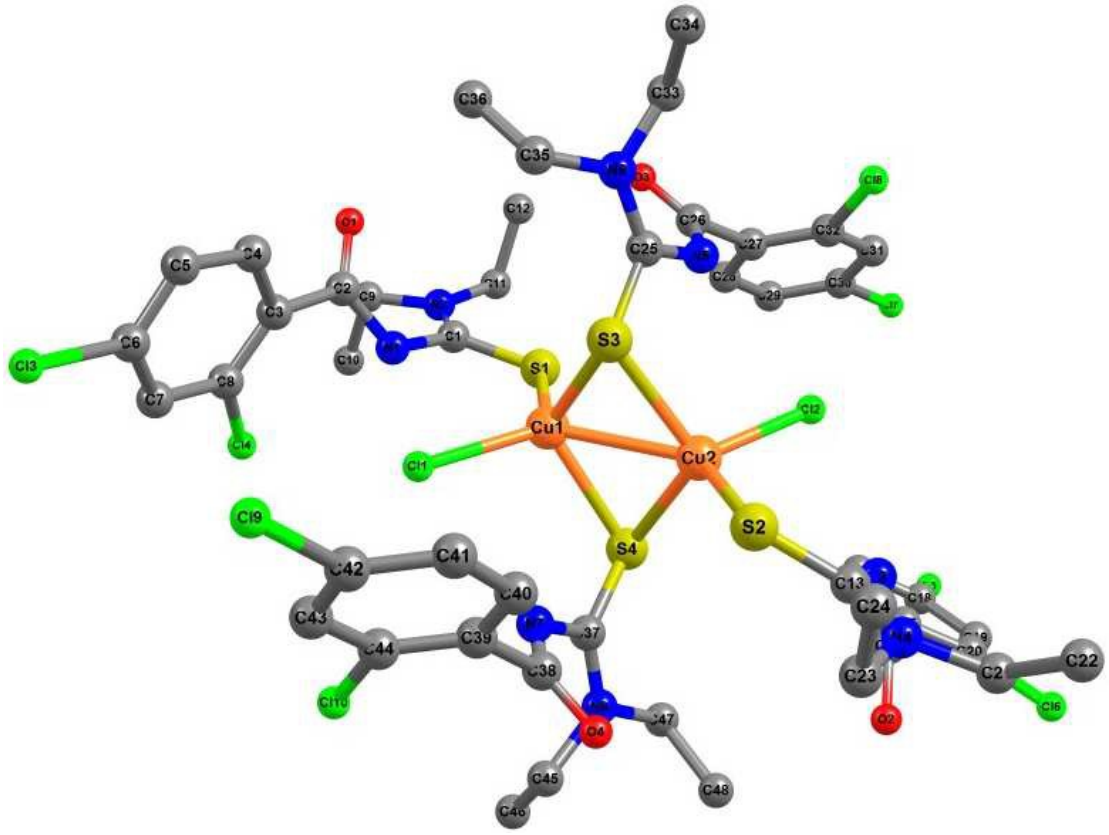

Fig. 6 Ground state optimized molecular structure of complex **1** (hydrogens are omitted for clarity).

This confirms that the S_0 state of the complex is more stable than the T_1 state. Since the Cu–Cu bond distance in complex 1 calculated at M06-2X level is only 0.09 Å higher than that calculated at B3LYP level, it is worth to note that the metal–metal bond is not significantly altered by the dispersion. Further, the pronounced energy difference of 17 kcal/mol between the B3LYP and M06-2X results accounts for the attractive dispersion interaction of the Cu metal centers with the surrounding organic ligands.

Frontier Molecular Orbital Properties: In order to characterize the electronic properties of **1**, the ground state electronic structure is discussed on the basis of frontier molecular orbital components, the HOMO and LUMO energy levels and energy gaps. The frontier molecular orbital composition of the complex is summarized in Table †S2 and the energy levels are illustrated in Fig. †S6. As shown in Fig. †S6, in the S_0 state, the HOMO is mainly localized on the metal centers, terminal chlorine and sulfur atoms, and the bridging sulfur ligands, whereas the LUMO is mainly localized on the ligand moieties (91%).

The isodensity surfaces of the Highest Singly Occupied Molecular Orbital (HSOMO) and Lowest Singly Occupied Molecular Orbital (LSOMO) and the corresponding spin density plot of complex **1** at T_1 state are shown in Fig. †S7. The analysis of the singly occupied molecular orbitals at the T_1 geometry shows that the HSOMO is mainly located on the metal center, terminal Cl ligands and the terminal and bridging sulfur atoms. This resembles the HOMO of the corresponding S_0 geometry. The LSOMO is mainly located on the metal center, terminal Cl ligand and the bridging sulfur atoms. The spin density at the T_1 geometry is mainly localized on the metal centers, terminal Cl ligand, bridging and terminal sulfur ligands, thus the lowest-lying triplet excited state has the ^{3}MLCT/^{3}ILCT character.

The HOMOs and LUMOs are often used to relate the spectral properties of complexes and provide decisive clues in designing new complexes. Therefore it is essential to identify and understand the nature of various segments of the complex and their individual contributions towards HOMOs and LUMOs. Hence, the contribution of various fragments of the complexes towards their HOMOs and LUMOs has been analyzed using QMForge Program.[57] The complex has been segmented into four fragments, namely metal centers (2Cu), terminal and bridging sulfur atoms (4S), terminal chlorine atoms (2Cl) and other parts of the ligand, and their corresponding percentage contributions are summarized in Table †S2. It can be found that the HOMO of the complex has a mixed Cu/S/π(ligand) character with different contributions. Table †S2 shows that the HOMO is mainly composed of 35.5% d(Cu), 39.7% p(S) and 19.7% π(ligand), whereas the LUMO is predominantly composed of π* orbital of the ligand (91%). The next five HOMOs (HOMO-1 to HOMO-5) are also composed of the mixed Cu/S/π(ligand) character with the main contributions from d(Cu), p(S) and π(ligand) and the LUMOs are predominantly π* orbital of the ligands. However, for LUMO+1 to LUMO+5 the main contribution (>86%) comes from π* orbital of the ligand. The above analysis reveals that the absorption spectrum is mainly associated with the ^{1}MLCT/^{1}ILCT character, which is in agreement with the experimentally obtained absorption spectrum.

Natural Bond Orbital Analysis: The net atomic charges of the selected atoms of complex **1** are calculated using Natural Population Analysis (NPA) and the results are summarized in Table †S3. NPA computes the charge that is transferred between the donor and acceptor moieties and this charge transfer indicates the type of bonding between the ligand and the metal. Table †S2 indicates the presence of electrovalent bonding between the Cu atoms and the ligand. The charge on both the Cu atoms is slightly lower than the formal charge. This is

due to the charge donation from the terminal and bridging S and terminal Cl atoms. The charge on the S donor center is significantly less negative than the charge on the terminal Cl atoms, indicating that there is higher electron density delocalization from the S atoms to Cu. In comparison with the S_0 state the metal centers in the T_1 state accept less charge from S and Cl atoms.

DNA Binding Studies

Changes in the electronic absorption spectra of the complexes (**1**–**4**) were chronicled as a function of DNA concentration, and the titration curves for the complexes are shown in Figs. 7 and †S8.

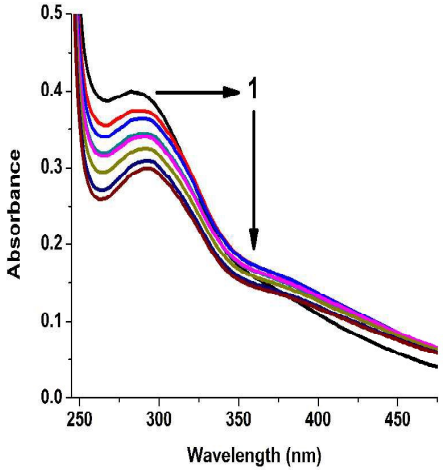

Fig. 7 Absorbance titrations of the complex **1** (5 μM) with CT DNA (0-50 μM).

There was a significant change in the absorption profile of **1**–**4** on sequential addition of DNA. The intrinsic binding constant of the complexes with CT DNA was determined from the equation[58] $[DNA]/(\varepsilon_a-\varepsilon_f) = [DNA]/(\varepsilon_b-\varepsilon_f) + 1/K_b(\varepsilon_b-\varepsilon_f)$, where [DNA] is the concentration of DNA in base pairs. The apparent absorption coefficients ε_a, ε_f, and ε_b correspond to A(observed)/[Cu], the extinction coefficient for the free complex and the extinction coefficient for the complex in the fully bound form, respectively. The slope and the intercept of the linear fit of $[DNA]/[\varepsilon_a-\varepsilon_f]$ *versus* [DNA] plot (Fig. †S9) gave $1/[\varepsilon_a-\varepsilon_f]$ and $1/K_b(\varepsilon_b-\varepsilon_f)$, respectively. The intrinsic binding constant (K_b) can be obtained from the ratio of the slope to the intercept. The binding constants for complexes **1**, **2**, **3** and **4** are 3.59×10^4, 3.16×10^4, 2.36×10^4 and 1.96×10^4 M^{-1} respectively (Table †S3). The absorption spectrum of **1** on addition of DNA showed 42% hypochromism with red shift ($\Delta\lambda$ = 7 nm) in the band corresponding to intra ligand transition (IL), while complex **2** showed 37% hypochromicity

with 5 nm red shift in the same band. For complex **3**, the hypochromism and red shift in the IL band are 34% and 3 nm respectively. The absorption spectra of **4** on addition of DNA showed 31% hypochromism and 7 nm red shift in the IL band. Compounds that bound to DNA through intercalation are characterized by a change in absorbance (hypochromism) and bathochromic shift, due to a π–π stacking interaction between the aromatic chromophore of the test compounds and DNA base pairs. The present spectral characteristics suggest that complex **1** showed better DNA binding propensity compared to the other complexes (**2**–**4**). Metal complexes with σ-bonded aromatic side arms can act as dual-function complexes: they bind to DNA both by metal coordination and through intercalation of the attached aromatic ligand. These aromatic side arms introduce new modes of DNA binding, involving mutual interactions of functional groups held in close proximity. DNA binding constant (K_b) value of the complexes (**1**–**4**) is comparable with that of the previously reported copper complexes.[59-62]

Relative binding of the Cu(II) complexes to CT DNA was studied by fluorescence spectral method using ethidium bromide (EB) bound CT DNA solution in Tris-HCl/NaCl buffer (pH 7.2). The fluorescence intensities of EB bounded DNA were recorded at 596 nm (510 nm excitation) with an increasing amount of the complex concentration. EB was non emissive in Tris-buffer medium due to fluorescence quenching of the free EB by the solvent molecules. [63,64] In presence of DNA, EB showed enhanced emission intensity due to its intercalative binding to DNA. A competitive binding of the Cu complexes to CT DNA resulted in the displacement of bound EB, and as a consequence, the emission intensity decreased. The emission spectra of EB-DNA in the presence and absence of the complexes (**1**-**4**) are shown in Fig.s 8 and †S10. The relative order of binding was obtained from the linear Stern-Volmer equation[65], $F^o/F = 1 + K_q[Q]$. Here, F^o and F are the fluorescence intensities in the absence and presence of the complexes, respectively, K_q is a linear Stern-Volmer quenching constant,

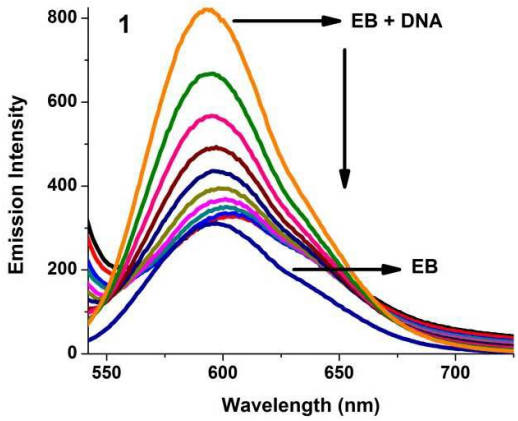

Fig. 8 Fluorescence titrations of the complex **1** (0-50 μM) with EB bounded CT DNA (5 μM).

and [Q] is the total concentration of a complex to that of DNA. The value of K_q is given by the ratio of slope to intercept in a plot of F^o/F *versus* [Q] (Fig. †S11). The quenching constant values are listed in Table †S4. The Stern-Volmer constant or quenching constant (K_q) is evaluated as 4.50×10^4, 4.14×10^4, 3.81×10^4 and 3.32×10^4 M^{-1} for complexes **1**, **2**, **3** and **4** respectively, which were in parity with the extent of displacement of ethidium bromide by the complexes. The apparent binding constant (K_{app}) values of the complexes were calculated by using the equation $K_{EB}[EB] = K_{app}[complex]$, where the complex concentration is the value at 50% reduction in the fluorescence intensity of EB and K_{EB} (1.0×10^7 M^{-1}) is the DNA binding constant of EB (Table †S4). The K_{app} value for **1**□**4** is 2.25×10^6, 2.07×10^6, 1.91×10^6 and 1.66×10^6 M^{-1}, respectively. The higher values of K_{app} establish the intercalation of copper complexes in to DNA major groove. The observed decrease in the emission intensity of EB-DNA (Fig.s 8 and †S10) and the DNA binding affinity of the complexes follow the order **1**>**2**>**3**>**4** (Table †S4). This is in conformity with the order of DNA binding affinity obtained from the absorption spectroscopy.

BSA Protein Interaction Studies

BSA protein consists of three aromatic amino acids, they are phenylalanine, tyrosine and tryptophan, and its fluorescence is due to tryptophan and tyrosine residues.[66] The interaction of the complexes (**1**–**4**) with BSA has been studied by using spectroflourometric method. Fig.s 9 and †S12 in show the variation in the emission of BSA with the addition of the copper

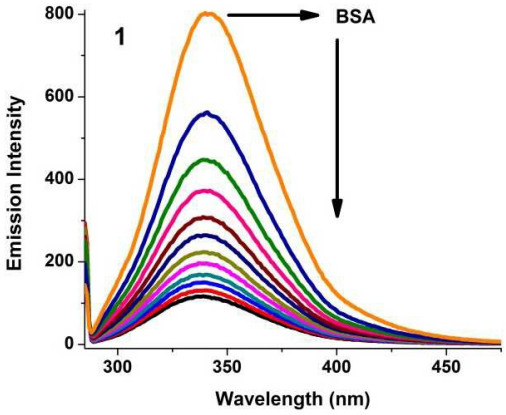

Fig. 9 Fluorescence titrations of the complex **1** (2 μM) with BSA (1 μM).

complexes (**1**–**4**). Fluorescence spectra were recorded in the range from 290 to 450 nm upon excitation at 280 nm. Upon the addition of the copper complexes to the solution of BSA, fluorescence intensity at 342 nm decreases up to 85.6, 72.2, 82.7 and 74.7% from the initial intensity of BSA accompanied by a hypsochromic shift of 6, 4, 3 and 5 nm for complexes **1**, **2**, **3** and **4** respectively. This quenching effect with red shift indicates the hydrophopic interaction of BSA protein with the complexes.[67,68] The fluorescence quenching data have been analyzed using the Stern-Volmer equation. The quenching constant (K_q) [2.21 × 10^5 (**1**), 1.41× 10^5 (**2**), 1.09 × 10^5 (**3**) and 9.24 × 10^4 (**4**)] can be calculated using the plot of F^o/F *versus* [Q] (Fig. †S13). At a certain point, when small molecules bind independently to a set of equivalent sites on a macromolecule, some will be in bound condition and some will be in unbound condition. So, the equilibrium between the unbound and bound molecules are represented by the following equation[69,70] $\log[(F^o–F)/F] = \log K_b + n \log[Q]$, where K_b [1.09 × 10^6 (**1**), 5.78× 10^5 (**2**), 3.36 × 10^5 (**3**) and 1.23 × 10^5 (**4**)] is the binding constant of the compound with BSA and n is the number of binding sites. From the plot of $\log[(F^o–F)/F]$ *versus* log[Q] (Fig. †S14), the number of binding sites (n) [1.18 (**1**), 1.11 (**2**), 1.09 (**3**) and 1.03 (**4**)] and the binding constant (K_b) values have been obtained. The calculated K_q, K_b and n values are given in Table †S5. The calculated value of n is around 1 for all of the complexes. The values of K_q and K_b suggested good interaction of the complexes with BSA. Among the four complexes, complex **1** exhibited better interaction with BSA. Interestingly, all the complexes showed higher BSA binding affinity than recently reported copper complexes.[71,72] N(4)-Phenyl substitution in the semicarbazone moiety and the change of the counterion (Cl^- or NO_3^-) in Cu(II) precursor affected the structure as well as the pharmacological properties of the complexes. These Cu(II)-semicarbazone complexes

possess more BSA binding property compared to **1**–**4** due to hydrophobic and electrostatic interactions.[73]

The mechanism of quenching is usually classified as dynamic and static. Static quenching refers to fluorophore-quencher complex formation in the ground state, and the dynamic quenching refers to a process in which the fluorophore and quencher come into contact during the transient existence of the excited state. The easiest method to determine the type of quenching is UV-Vis absorption spectroscopy. The UV-Vis spectra of BSA in the absence and presence of the complexes are shown in Fig. 10. The addition of the Cu complexes to a fixed concentration of BSA led to a gradual increase in the intensity of BSA absorption at the same wavelength due to the interaction between the complexes and protein, which is mainly ascribed to the static quenching.[74]

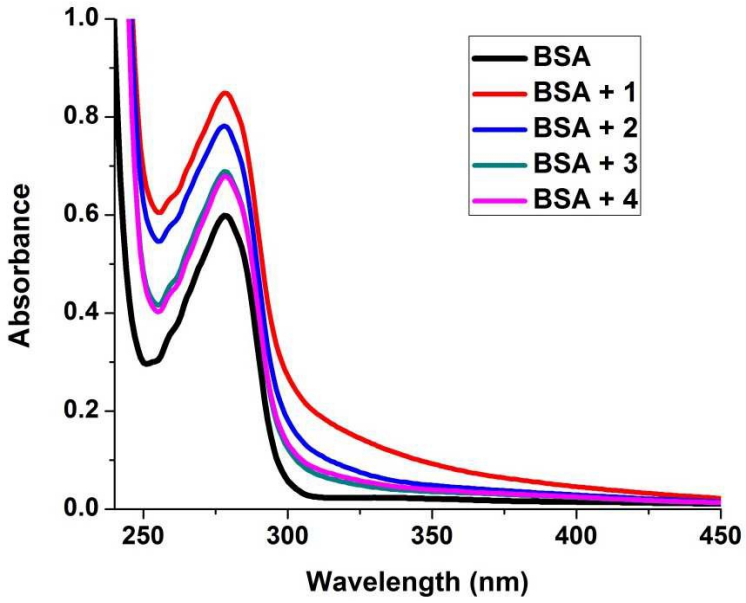

Fig. 10 Absorbance titration of the complexes with BSA.

In synchronous fluorescence spectroscopy, according to Miller[75], the difference between excitation and emission wavelengths reflects the spectra of a different nature of chromophores. With large Δλ values such as 60 nm, the synchronous fluorescence of BSA is characteristic of the tryptophan (Fig.s 11A and †S15) residue and small Δλ value such as 15 nm is characteristic of tyrosine[76] (Fig.s 11B and †S16). To understand the structural changes in BSA protein due to the addition of the complexes (**1**–**4**) we have measured synchronous

fluorescence spectra. While increasing the concentration of the complexes, the intensity of

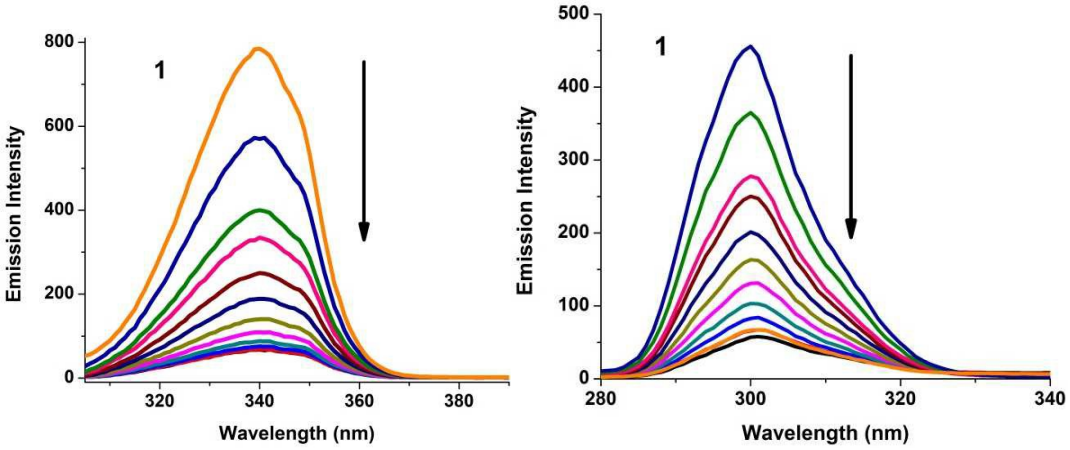

A **B**

Fig. 11 Synchronous spectra of BSA (1 μM) as a function of concentration of the complex **1** (0-20 μM) with Δλ = 60 nm **(A)** and Δλ = 15 nm **(B)**.

emission corresponding to tyrosine (at 300 nm) was found to decrease in the magnitude of 87.0, 60.1, 80.8 and 69.7% for complexes **1**, **2**, **3** and **4** respectively without any shift in their emission wavelength. The tryptophan fluorescence emission showed significant decrease in the intensity (at 340 nm) [91.5 (**1**), 65.4 (**2**), 83.1 (**3**) and 70.6% (**4**)] without any change in the position of the emission band. These experimental results indicate that although the complexes affected the micro environments of both tyrosine and tryptophan during the binding process, the effect is more pronounced towards tryptophan than tyrosine. Hence, the results clearly indicate that the complexes bind to the active sites in the protein, which make them potential molecules for biological applications.

Cytotoxicity

The *in vitro* cytotoxicity of the Cu(II) complexes was determined against human A549 (human lung adenocarcinoma epithelial cell line) and MCF7 (human breast cancer cell line) cells by means of the colorimetric MTT assay and compared to the activity of the commercially available drug cyclophosphamide. Media (DMSO/buffer) and cyclophosphamide were used as controls under the same experimental conditions. The resulting 50% growth inhibitory concentration (IC50) values are summarized in Table S6 in the ESI and graphically depicted in Fig.s †S17 and †S18. Complexes **1** [IC50 = 63.73 (A549); 70.71 (MCF7)] and **4** [IC50 = 50.00 (A549); 20.45 (MCF7)] showed comparable cytotoxic activity with cyclophosphamide [IC50 = 41.84 (A549); 11.89 (MCF7)] at both low and high micro molar concentrations. Compound **4** showed remarkable cytotoxicity against

both the cancer cell lines after 24 h incubation. Its activity is more than that of **1**, **2** [IC50 = 103.85 (A549); 81.69 (MCF7)] and **3** [IC50 = **1**60.85 (A549); 155.44 (MCF7)]. However cytotoxicity of the complexes (**1**–**4**) is comparable with that of previously reported copper complexes[77–79] comprising N-((1H-imidazole-2-yl)methyl)-2-(pyridine-2-yl)ethanamine/ meclofenamic acid/N,N′-tetra(4-antipyrylmethyl)-1,2-diaminoethane against A549 and MCF7 cancer cell lines.[80] Copper complexes of bis-β-diketone-type ligand (the curcumine derivative) have been used as a fluorescent probe, but it did not show significant cytotoxic activity against A549, HeLa and MCF-7 cell lines.[81] Copper complexes containing 2,2-bis(3,5-dimethyl-1H-pyrazol-1-yl)-N-(2-(2-methyl-5-nitro-1H-imidazol-1-yl)ethyl)acetamide and 1,3,4,6-tetra-O-acetyl-2-{[bis(3,5-dimethyl-1H-pyrazol-1-yl)-acetyl]amino}-2-deoxy-β-D-glucopyranose showed more cytotoxic activity (IC50 = 7−14 μM) than complexes **1**–**4** against MCF7 and A549 cancer cell lines.[82]

Conclusions

Reactions of HL1 and HL2 with $CuCl_2{\cdot}2H_2O$ yielded complexes **1** and **3** respectively. Analogous reaction between HL1 / HL2 and copper(II) acetate yielded **2** / **4**. The structure of all the complexes was confirmed by the single crystal X-ray diffraction method and is supported by analytical and spectroscopic data. Furthermore, to elucidate the structural and bonding properties of complex **1**, density functional theory calculations were performed. Close agreement was found between the X-ray crystallographic data and those determined by the computational methods. Frontier molecular orbital analyses reveal that the absorption spectrum is mainly associated with the metal to ligand charge transfer character. The results of the singly occupied molecular orbital at the T_1 geometry show that highest singly occupied molecular orbital resembles the highest occupied molecular orbital and lowest singly occupied molecular orbital resembles the lowest unoccupied molecular orbital of the corresponding S_0 geometry. The spin density at the T_1 geometry is mainly localized on the metal centers, terminal Cl ligand, and bridging and terminal sulfur ligands, thus the lowest-lying triplet excited state has metal to ligand charge transfer character. The DNA and protein binding affinities and cytotoxic activity of the complexes were described. Interestingly complex **1** showed higher binding affinity with CT DNA as well as with BSA protein. All the complexes displayed significant toxicity against A549 and MCF7 cancer cell lines. Particularly cytotoxicity of **1** and **4** is comparable with cyclophosphamide.

Acknowledgements

N.S. thanks NITT for the fellowship. R.K. gratefully acknowledges DST for the financial support.

References

1 G. Zuber, J. C. Jr. Quada and S. M. Hecht, *J. Am. Chem. Soc*., 1998, **120**, 9368–9369.

2 S. M. Hecht, *J. Nat. Prod*., 2000, **63**, 158–168.

3 C. Cardin and J. Hall, *Nature Chemistry*, 2012, *4*, 587.

4 B. M. Zeglis, V. C. Pierre and J. K. Barton, *Chem. Commun*., 2007, 4565–4579.

5 C. Metcalfe and C. Thomas, *J. A. Chem. Soc. Rev*., 2003, **32**, 215–224.

6 K. E. Erkkila, D. T. Odom and J. K. Barton, *Chem. Rev*., 1999, **99**, 2777–2796.

7 D. S. Sigman, A. Mazumder and D. M. Perrin, *Chem. Rev*., 1993, **93**, 2295–2316.

8 T. J. Peters, *Adv. Protein Chem*., 1985, **37**, 161–245.

9 J. R. Brown, *Albumin Structure, Function and Uses*; V. M. Rosenoer, M. Oratz, M. A. Rothschild, (Eds.), Pergamon, Oxford, U.K., Vol. **27**, 1977.

10 T. J. Peters, *All About Albumin*, Academic Press, San Diego, CA, 1996.

11 X. M. He and D. C. Carter, *Nature*, 1992, **358**, 209–215.

12 M. K. Helms, V. Paterson, N. V. Bhagavan and D. M. Jameson, *FEBS Lett*., 1997, **408**, 67–70.

13 Y. Suzuki and K. Yokoyama, *J. Am. Chem. Soc*., 2005, **127**, 17799–17802.

14 A. Mallick, B. Halder and N. Chattopadhyay, *J. Phys. Chem*., B 2005, **109**, 14683–14690.

15 R. Das, D. Guha, S. Mitra,; S. Kar, S. Lahiri and S. Mukherjee, *J. Phys. Chem*. A, 1997, **101**, 4042–4047.

16 N. Selvakumaran, N. S. P. Bhuvanesh, A. Endo and R. Karvembu, *Polyhedron*, 2014, **75**, 95–109.

17 N. Selvakumaran, N. S. P. Bhuvanesh and R. Karvembu, *Dalton Trans*., 2014, 43, 16395–16410.

18 J. Lang and K. Tatsumi, *Polyhedron*, 1996, **15**, 2127–2130

19 X. Gua, Z. Shia, J. Penga, Y. Chena, E. Wanga and N. Hu, *J. Mol. Struct*., 2004, **694**, 219–222.

20 M. Belicchi-Ferrari, F. Bisceglie, E. Buluggiu, G. Pelosi and P. Tarasconi, *Polyhedron*, 2009, **28**, 1160–1168.

21 C. Näther, J. Greve, I. Jeß and C. Wickleder, *Solid State Sci*., 2003, **5**, 1167–1176.

22 J. Xiang-Lin, J. Yi-Yan and T. You-Qi, *Acta Chim. Sinica*, 1986, **44**, 580–583.

23 T. Ka-Luo, J. Xiang-Lin, L. Yu, L. Yao-Ling, C. Peng and T. You-Qi, *Acta Chim. Sinica*, 2000, **58**, 866–870.

24 K. Johnson and J. W. Steed, *J. Chem. Soc. Dalton Trans*., 1998, 2601–2602.

25 P. K. Bharadwaj,; E. John, C. L. Xie,; D. Zhang, D. N. Hendrickson, J. A. Potenza and J. H. Schugar, *Inorg. Chem*., 1986, **25**, 4541–4546.

26 G. A. Bowmaker, J. V. Hanna, C. Pakawatchai, B. W. Skelton, Y. Thanyasirikul and A. H. White, *Inorg. Chem*., 2009, **48**, 350–368.

27 P. Gary Eller and P. W. R. Corfie, *Chem. Commun*., 1971, 105–106.

28 M. M. Ibrahim, S. Y. Shaban, *Inorg. Chim. Acta*, 2009, **362**, 1471–1477.

29 M. Jake Pushie, L. Zhang, I. J. Pickering and N. G. Graham, *J. Inorg. Biochem*. 2000, **82**, 229–238.

30 W. Minder and E. Z. Stocker, *Kristallogr*. 1936, **94**, 137–141.

31 K. R. Koch, J. du Troit, M. R. Caira and C. Sacht, *J. Chem. Soc. Dalton Trans*., 1994 785−786.

32 W. Hernandeza, E. Spodinea, A. Vegab, R. Richterc, J. Griebelc, R. Kirmsec, U. Schröderc and L. Beyer, *Z. Anorg. Allg. Chem*., 2004, **630**, 1381−1386.

33 H. Arslan, U. Florke, N. Kulcu and M. F. Emen, *J. Coord. Chem*., 2006, **59**, 223–228.

34 APEX2 "Program for Data Collection and Integration on Area Detectors" BRUKER AXS Inc. 5465 East Cheryl Parkway, Madison WI 53711−53731 USA.

35 G. M. Sheldrick, "TWINABS (version 2008/1): *Program for Absorption Correction for Data from Area Detector Frames*", University of Göttingen 2008.

36 G. M. Sheldrick, *Acta Cryst*. A, 2008, **64**, 112−122.

37 O. V. Dolomanov, L. J. Bourhis, R. J. Gildea, J. A. K. Howard and H. Puschmann, *J. Appl. Cryst*., 2009, **42**, 339–341.

38 A. D. Becke, *J. Chem. Phys*., 1993, **98**, 5648–5652.

39 C. Lee, W. Yang and R. G. Parr, *Phys. Rev*. B: *Condens*. *Matter*, 1988, **37**, 785−789.

40 P. J. Hay and W. R. Wadt, *J. Chem. Phys*., 1985, **82**, 299–310.

41 Jaguar. 6.5, v. E. Schroedinger, LLC: New York 2005.

42 Y. Zhao and D. G. Truhlar, *Theor. Chem. Acc*., 2008, **120**, 215.

43 Y. Zhao and D. G. Truhlar, *Acc. Chem. Res*., 2008, **41**, 157.

44 M. J. Frisch, G. W. Trucks, H. B. Schlegel, G. E. Scuseria, M. A. Robb, J. R. Cheeseman, G. Scalmani, V. Barone, B. Mennucci, G. A. Petersson, H. Nakatsuji, M. Caricato, X. Li, H. P. Hratchian, A. F. Izmaylov, J. Bloino, G. Zheng, J. L. Sonnenberg, M. Hada, M. Ehara, K. Toyota, R. Fukuda, J. Hasegawa, M. Ishida, T. Nakajima, Y. Honda, O. Kitao, H. Nakai, T. Vreven, J. A. Jr. Montgomery, J. E. Peralta, M. Bearpark,

J. J. Heyd, E. Brothers, K. N. Kudin, V. N. Staroverov, R. Kobayashi, J. Normand, K. Raghavachari, A. Rendell, , J. C. Burant; S. S. Iyengar, J. Tomasi, M. Cossi, N. Rega, J. M. Millam, M. Klene, J. E. Knox, J. B. Cross, V. Bakken, C. Adamo, J. Jaramillo, R. Gomperts, R. E. Stratmann, O. Yazyev, A. J. Austin, R. Cammi, C. Pomelli, J. W. Ochterski, R. L. Martin, K. Morokuma, V. G. Zakrzewski, G. A. Voth, P. Salvador, J. J. Dannenberg, S. Dapprich, A. D. Daniels, O. Farkas, J. B. Foresman, J. V. Ortiz, J. Cioslowski and D. J. Fox, *Gaussian*, *Inc*. Wallingford CT 2009.

45 T. K. Goswami, B. V. Chakravarthi, M. Roy, A. A. Karande and A. R. Chakravarty, *Inorg. Chem*., 2011, **50**, 8452–8464.

46 C. J. Doona and D. M. Stanbury, *Inorg. Chem*., 1996, **35**, 3210–3216.

47 A. B. P. Lever, (2nd ed.), *Inorganic Electronic Spectroscopy*, Elsevier, Amsterdam, 1984.

48 L. X. Chen, G. B. Shaw, I. Novozhilova, T. Liu, G. Jennings, K. Attenkofer, G. J. Meyer and P. Coppens, *J. Am. Chem. Soc*., 2003, **125**, 7022–7034.

49 D. J. Che, G. Li, X. L. Yao, Y. Zhu and D. P. Zhou, *J. Chem. Soc. Dalton Trans*., 1999, 2683–2687.

50 R. C. Aggarwal, N. K. Singh and R. P. Singh, *Inorg. Chem*., 1981, **20**, 2794–2798.

51 A. W. Addison, R. T. Nageswara, J. Reedijk, J. Rijn and G. J. Verschoor, *J. Chem. Soc. Dalton Trans*., 1984, 1349.

52 K. D. Karlin, R. W. Cruse, Y. Gultneh, A. Farooq, J. C. Hayes and J. Zubieta, *J. Am. Chem. Soc*., 1987, **109***,* 2668–2679.

53 L. Yang, D. R. Powell and R. P. Houser, *Dalton Trans*., 2007, 955–964.

54 E. Constable, C. E. Housecroft, B. M. Kariuki, N. Kelly and C. B. Smith, *Comptes Rendus Chimie*, 2002, *5*, 425–430.

55 R. Das, D. Guha, S. Mitra, S. Kar, S. Lahiri and S. Mukherjee, *J. Phys. Chem*. A, 1997, **101**, 4042−4047.

56 S. Mahapatra, J. A. Halfen, E. C. Wilkinson, G. Pan, X. Wang, V. G. Jr. Young, C. J. Cramer, L. Jr. Que and W. B. Tolman, *J. Am. Chem. Soc*., 1996, **118**, 11555−11574.

57 A. Tenderholt, QMForge, *A Program to Analyze Quantum Chemistry Calculations*, Version 2.3.2.

58 A. Wolfe, G. H. Shimer and T. Meehan, *Biochemistry*, 1987, **26**, 6392–6396.

59 R. Loganathan, S. Ramakrishnan, E. Suresh, M. Palaniandavar, A. Riyasdeen, M. A. Akbarsha, *Dalton Trans*., 2014, **43**, 6177–6194.

60 E. Sundaravadivel, S. Vedavalli, M. Kandaswamy, B. Varghese and P. Madankumar, *RSC Adv*., 2014, **4**, 40763–40775.

61 M. Belicchi-Ferrari, F. Bisceglie, G. Pelosi and P. Tarasconi, *Polyhedron*, 2008, **27** 1361.

62 D. S. Raja, G. Paramaguru, N. S. P. Bhuvanesh, J. H. Reibenspies, R. Renganathan and K. Natarajan, *Dalton Trans*., 2011, **40**, 4548.

63 M. J. Waring, *J. Mol. Biol*. 1965, **13**, 269–282.

64 I. Changzheng, W. Jigui, W. Liufang, R. Min, J. Naiyang and G. Jie, *J. Inorg. Biochem*. 1999, **73**, 195–202.

65 M. Lee, A. L. Rhodes, M. D. Wyatt, S. Forrow and J. A. Hartley, *Biochemistry*, 1993, **32**, 4237–4245.

66 K. A. Z. Osama and I. Othman, *J. Am. Chem. Soc*., 2008, **130**, 10793−10801.

67 Q. Wang, L. Lu, C. Yuan, K. Pei, Z. Liu, M. Guo and M. Zhu, *Chem. Commun*., 2010, **46**, 3547–3549.

68 D. S. Raja, N. S. P. Bhuvanesh and K. Natarajan, *Eur. J. Med. Chem*., 2011, **46**, 4584–4594.

69 J. R. Lakowicz, *Fluorescence Quenching: Theory and Applications*. *Principles of Fluorescence Spectroscopy*, Kluwer Academic/PlenumPublishers, New York, 1999, pp 53−127.

70 X. Z. Feng, Z. Yang, L. J. Wang and C. Bai, *Talanta* 1998, **47**, 1223−1229.

71 J. Lu, Q. Sun, J. L. Li, L. Jiang, W. Gu, X. Liu, J. L. Tian and S. P. Yan, *J. Inorg. Biochem*., 2014, **137**, 46–56.

72 A. Patra, T. K. Sen, A. Ghorai, G. T. Musie, S. K. Mandal and U. Ghosh, *Inorg. Chem*., 2013, **52**, 2880–2890.

73 D. S. Raja, N. S. P. Bhuvanesh and K. Natarajan, *Inorg. Chem*., 2011, **50**, 12852.

74 P. Krishnamoorthy, P. Sathyadevi, A. H. Cowley, R. R. Butorac and N. Dharmaraj, *Eur. J. Med. Chem*., 2011, **46**, 3376–3387.

75 J. N. Miller, *Proc. Anal. Div. Chem. Soc*., 1979, **16**, 203–208.

76 J. H. Tang, F. Luan and X. G. Chen, *Bioorg. Med. Chem*., 2006, **149**, 3210–3217.

77 P. Kumar, S. Gorai, M. K. Santra, B. Mondal and D. Manna, *Dalton Trans*., 2012, **41**, 7573–7581.

78 D. Kovala-Demertzi, M. Staninska, I. Garcia-Santos, A. Castineiras and M. A. Demertzis, *J. Inorg. Biochem*., 2011, **105**, 1187–1195.

79 E. M. Mosoarca, I. Pantenburg, R. Tudose, G. Meyer, N. C. Popa, A. Han, R. Alexandrova, R. Kalfin, W. Linert and O. Costisor, *Inorg. Chim. Acta*, 2011, **370**, 460–468.

80 S. S. Zhou, X. Xue, B. Jiang and Y. P. Tian, *Sci. China. Chem*., 2012, **55**, 334.

81 M. Pellei, G. Papini, A. Trasatti, M. Giorgetti, D. Tonelli, M. Minicucci, C. Marzano, V. Gandin, G. Aquilanti, A. Dolmella and C. Santini, *Dalton Trans*., 2011, **40**, 9877.

82 S. A. Galal, K. H. Hegab, A. S. Kassab, M. L. Rodriguez, S. M. Kerwin, A.-M. m. A. El-Khamry and H. I. El Diwani, *Eur. J. Med. Chem*., 2009, **44**, 1500.

"For Table of Contents Only"

Structural Diversity in Aroylthiourea Copper Complexes – Formation and Biological Evaluation of $[Cu(I)(\mu\text{-}S)SCl]_2$, *cis*-$Cu(II)S_2O_2$, *trans*-$Cu(II)S_2O_2$ and $Cu(I)S_3$ cores

Nagamani Selvakumaran, Lakshmanan Sandhiya, Nattamai S.P. Bhuvanesh, Kittusamy Senthilkumar, Ramasamy Karvembu

Four different copper complexes containing aroylthiourea ligands displayed good interaction with CT DNA and BSA and cytotoxicity.